ASIC1a is required for neuronal activation via low-intensity ultrasound stimulation in mouse brain

Jormay Lim, Ya-Cherng Chu, Chen-Ming Hao, Wei-Hao Liao, Shao-Shien Lin, Sherry Hsu, Hsiao-Hsin Tai, Ya-Chih Chien, Dar-Ming Lai, Wen-Shiang Chen, Chih-Cheng Chen* and Jaw-Lin Wang*

Jormay Lim, Ya-Cherng Chu, Chen-Ming Hao and Wei-Hao Liao contribute equally.

Address correspondence and requests for reprints to

*Jaw-Lin Wang, Ph.D., corresponding author

Professor, Department of Biomedical Engineering, College of Medicine and College of Engineering, National Taiwan University,

Address: 602 Jen-Su Hall, 1 Section 4, Roosevelt Road, Taipei 10617, Taiwan, ROC

Phone: 886-2-33665269, Fax: 886-2-23687573, Email: jlwang@ntu.edu.tw

*Chih-Cheng Chen, Ph.D. corresponding author

Research fellow, Institute of Biomedical Sciences, Academia Sinica

Address: 128 Academia Road, Section 2, Taipei 115, Taiwan

Phone: 886-2-26523917, Fax: 886-2-27829224, Email: chih@ibms.sinica.edu.tw

ACKNOWLEDGEMENT

This study was supported by Ministry of Science and Technology, Taiwan (MOST 107-2221-E-002-068-MY3, MOST108-2321-B-002-047, MOST 108-2321-B-002-061-MY2), National Health Research Institute, Taiwan (NHRI-EX109-10924EI), National Taiwan University (NTU-CC-107L891105); and a grant from MOST, Taiwan (MOST 108-2321-B-001-028-MY2) to CCC.

SIGNIFICANCE

CNS neurons have no sensory function, protected by the skull. For this reason, brain neuromodulation by ultrasound were either done at a high intensity or through auditory nerves. We demonstrate in this study CNS neurons react to ultrasound stimulation at an intensity (5 mW/cm^2) far lower than typical therapeutic ultrasound (>30 mW/cm^2). Using micropipette ultrasound in calcium imaging, we show the reactions of CNS neurons to ultrasound is through ASIC1a channels, pointing to the molecular basis for direct ultrasound neuromodulation at low intensity. Furthermore, we also show evidence of neurogenesis with the same ultrasound stimulation, suggesting potential therapeutic translation.

ABSTRACT

Accumulating evidence has shown transcranial low-intensity ultrasound can be potentially a non-invasive neural modulation tool to treat brain diseases. However, the underlying mechanism remains elusive, because the majority of studies on animal models applying rather high-intensity ultrasound that cannot be safely used in humans. Here we showed low-intensity ultrasound was able to activate neurons in the mouse brain and repeated ultrasound stimulation resulted in adult neurogenesis in specific brain regions. *In vitro* calcium imaging studies showed that a specific ultrasound stimulation mode, which combined with both ultrasound-induced pressure and acoustic streaming mechanotransduction, is required to activate cultured cortical neurons. ASIC1a and the tether-mode mechanotransduction were involved in the low-intensity ultrasound-mediated mechanotransduction and cultured neuron activation, which was inhibited by ASIC1a blockade and cytoskeleton-modified agents. In contrast, the inhibition of mechanical sensitive channels involved in bilayer-model mechanotransduction like Piezo or TRP proteins did not affect the ultrasound-mediated neuronal activation.

53 **Introduction**

54 Transcranial ultrasound such as opening blood-brain barrier (BBB) (1) for
55 localized drug release and modulating neural activity (2-4) has been used for
56 therapeutic treatments of various brain diseases. Many *in vivo* animal experiments
57 and human clinical trials (*SI Appendix,* Table 1) proved the clinical potential of
58 transcranial ultrasound stimulation. With the increased interest of this technique, the
59 mechanisms underlying ultrasound-mediated neural modulation has also recently
60 been learned. A study showed high-intensity transcranial ultrasound can elicit a
61 startle-like motor response via an indirect auditory mechanism (5). Emerging
62 sonogenetics in worm model also identified and engineered TRP-4 channels as a
63 sensor for the ultrasound stimulus to activate neurons in living organisms at pressure
64 level above 0.5 MPa (6), and ultrasound at 0.1 MPa acoustic pressure was found to
65 activate neurons via Piezo 1 mechanosensitive ion channel (7). Nonetheless, the
66 energy intensity or acoustic pressure of most clinical trials or basic researches used
67 for BBB opening or neuromodulation are both high, and safety issue of this
68 technique in clinical application remains a concern.

69 In this study, a much lower intensity ultrasound at the order lower than 10
70 mW/cm^2 is proposed to activate neurons via mechanosensitive ion channels in
71 mammals' brain for potential clinical application. Mechanosensitve ion channels are
72 mainly grouped into bilayer model, such as PIEZO and TRP channels gated by
73 membrane tension change, and extracellular matrix tethered model such as acid
74 sensing ion channels (ASICs) (8-10). Here we aim to identify possible mechanical
75 sensors in mouse brain that can directly respond to low-intensity ultrasound.

76

77 **Results**

78 **Transcranial ultrasound induced p-ERK in the cortex, hippocampus and amygdala of**

79 **mouse brain.** We kept ultrasound exposure to below 10 mW/cm^2 (I_{SATA}) in our
80 experiments to ensure safe therapeutic applicability. The phosphorylation of
81 extracellular-signal-regulated kinase (p-ERK), an established indicator of immediate
82 neuronal activation (11), was used to evaluate whether transcranial low-intensity
83 ultrasound can stimulate neuronal activity in mouse brain. Mice with 1-minute
84 ultrasound exposure (Fig. 1 *A*) had shown significant increase of p-ERK positive cells in
85 certain brain regions, such as the cortex (Fig. 1 *B-D*), hippocampus (Fig. 1 *E-G*), and
86 amygdala (Fig. 1 *H-J*) as compared with those received sham treatment (*SI Appendix,*
87 Table 2). More specifically, increased p-ERK expression generally occurred upon
88 ultrasound stimulation in the visual, somatosensory, auditory, temporal associations,
89 retrosplenial, piriform, and entorhinal areas of mouse cortex (*SI Appendix,* Fig. S1 and
90 S2). In hippocampus, CA1 and CA2 were dramatically lightened up with p-ERK signals
91 in response to ultrasound whereas CA3 and dentate gyrus showed sparsely stimulated
92 (*SI Appendix,* Fig. S1 and S2). In amygdala, the central amygdala nucleus showed the
93 strongest p-ERK signals, while medial and basolateral also obviously increased in p-ERK
94 signals (*SI Appendix,* Fig. S1 and S2). We also observed a consistently unchanged p-ERK
95 staining in the paraventricular nucleus of hypothalamus (PVH) (*SI Appendix,* Fig. S3),
96 revealing an intriguing regional specificity of the ultrasound response.
97 **Micropipette guided ultrasound as the mechanical stimuli with combined ultrasound**
98 **and acoustic streaming.** To determine whether low-intensity ultrasound can directly
99 activate neurons mechanically, we next used in vitro calcium-imaging approach to
100 probe the possible ion channels responding to ultrasound mechanical stimulus in
101 cultured cortical neurons. A micropipette was used to guide ultrasound to cultured
102 cells (Fig. 2 *A*). The device can generate either an ultrasound induced pressure
103 predominant condition (2000 mVpp, DF 0.05%, measured peak pressure versus the
104 distance to the pipette tip shown in *SI Appendix,* Fig. S4 *A*) or an acoustic streaming

105 predominant condition (100 mVpp, DF 100%, flow pattern for the acoustic streaming
106 shown in *SI Appendix,* Fig. S4 *A* and Movie S1), or a mixed loading condition (700 mVpp,
107 DF 20%) depending on duty cycle applied. Ultrasound pressure predominant
108 conditions (up to 2000 mVpp, DF 0.05%) generated compressional stress on cells that
109 were not able to elevate calcium responses (Fig. 2 *B* and *SI Appendix,* Movie S2), while
110 acoustic streaming predominant conditions (up to 100 mVpp, DF 100%) invoked shear
111 stress that could only activate little calcium responses in neurons in the maximal
112 energy level applied (Fig. 2 *B*); whereas a mixed loading condition (700 mVpp, 20% DF)
113 effectively yielded much higher calcium responses (Fig. 2 *B* and *SI Appendix,* Movie S3).
114 The ultrasound predominant mode with only compressional stress cannot induce a
115 response even when the stimulation was extended to 10 seconds (*SI Appendix,* Fig. S5
116 *A*). Similarly, the prolong stimulation of acoustic streaming invoking shear stresses also
117 only elevated mildly the amplitude of calcium response (*SI Appendix,* Fig. S5 *B*). On the
118 other hand, the combined compression stress with acoustic streaming can
119 reproducibly elevated calcium response even in 1.5 second stimulation (Fig. 2 *B* and *SI*
120 *Appendix,* Movie S3, Fig. S5 *C*). The ultrasound-induced calcium responses were dose-
121 dependent with a threshold of 400 mVpp (8 kPa) and EC_{50} of 700 mVpp (12kPa) (Fig. 2
122 *C* and *SI Appendix* Fig. S5 *D-K*). The corresponding stress levels of ultrasound at 400
123 mVpp, 500 mVpp, 700 mVpp or 900 mVpp were 8 kPa, 8.72 kPa, 12 kPa and 15.3 kPa,
124 respectively.

125 **Neuronal calcium signal upon ultrasound simulation suppressed by ASIC channels**
126 **inhibitors.** The micropipette ultrasound mechanotransduction was pharmacologically
127 tested with selective or non-selective blockers of mechanosensitive ion channels for
128 Piezo, TRP, and ASICs. First, the treatment with Gadolinium (10 μM), a non-selective
129 blocker of mechanically sensitive ion channels, partially suppressed the ultrasound-
130 induced calcium signals (Fig. 2 *D*). Treating the cells with a selective Piezo inhibitor,

131 GsMTx-4, led to a marginal (not significant) inhibition of the ultrasound-induced
132 calcium elevation as compared with the vehicle control (Fig. 2 *E*). Instead, the
133 treatment with a TRP blocker ruthenium red (1-10 μM) partially suppressed the
134 calcium signals (Fig. 2 *F*), whereas the non-selective ASIC inhibitor, amiloride, totally
135 abolished the calcium signals by micropipette ultrasound (Fig. 2 *G*). Above results
136 suggested ASICs might be the major channels involved in micropipette ultrasound
137 mechanotransduction. To narrow down the specific candidate of ASICs, ASIC1a
138 inhibitor, PcTx1 (50nM) was tested. PcTx1 (50 nM) significantly inhibited the calcium
139 response by micropipette ultrasound (Fig. 2 *H* and *SI Appendix,* Fig. S5 *C*). The relative
140 inhibitions of above channel blockers were summarized in Fig. 2*I*. We further tested
141 the dose-dependent inhibition of PcTx1 on micropipette ultrasound and determined
142 an IC50 of 0.2nM, suggesting a homotrimeric ASIC1a is the mechanoreceptor in
143 action (Fig. 3 *A* and *SI Appendix,* Fig. S6 *A-F*). To validate how ASIC1a activation would
144 lead to calcium responses to ultrasound, we treated the cells with calcium chelating
145 agent, ethylene glycol-bis(β-aminoethyl ether)-N,N,N′,N′-tetraacetic acid (EGTA) (1-
146 5mM) to block the extracellular calcium. The results showed that calcium influx was
147 absolutely essential (Fig. 3 *B* and *SI Appendix,* Fig. S6 *G* and *H*). To examine whether
148 endoplasmic reticulum calcium was involved in calcium signaling, we found the
149 calcium surge of cells treated with the RyR inhibitor, JTV519 fumarate (10 μM) (*SI*
150 *Appendix,* Fig. S6 *G* and *I*) was partially inhibited, while as the IP3R inhibitor, (-)-
151 Xestonspongin C (1 μM) was most inhibited (Fig. 3 *B*).
152 **ASIC1a mechano-response required cytoskeletal dynamics.** Previous studies have
153 shown ASICs are involved in tether mode mechanotransduction, which relies on
154 intact cytoskeletal structures (8, 12). We likewise treated the cells with either actin
155 polymerization inhibitor, cytochalasin D (5-10 μg/ml) or microtubule assembly
156 inhibitor, nocodazole (5-10 μg/ml). Indeed, inhibition of cytoskeletal dynamics could

157 dose dependently and significantly suppress the calcium response stimulated by
158 micropipette ultrasound (Fig. 3 *C-E*). The collated data revealed a novel mode of
159 ultrasound mechanotransduction with a combination of compression force and shear
160 force that activates ASIC1a channels in mouse neurons via tether mode
161 mechanotransduction (Fig. 3 *F*).
162 **Transcranial ultrasound treatments promoted neurogenesis in dentate gyrus.** We
163 next investigated whether the low-intensity ultrasound stimulation in mouse brain
164 could lead to a favorable outcome in terms of adult neurogenesis. We selected
165 doublecortin (DCX) as a marker for neurogenesis in dentate gyrus (13-15). Compared
166 to the non-treated controls, after 3 consecutive days of 5 minute ultrasound
167 treatments (5 mW/cm^2), DCX staining in dentate gyrus at day 4 and day 7 showed a
168 significant 2-fold increase (Fig. 4). The results indicated that repeated stimulation of
169 low-intensity ultrasound on mouse brain might achieve beneficial neural modulation
170 and lead to neurogenesis in dentate gyrus.
171
172 **Discussion**
173 Accumulating evidence has shown ASICs are involved in different types of
174 mechanotransduction in the sensory nervous system, including nociception,
175 barorecpetion, proprioception, and hearing (8, 16, 17). However, the
176 mechanosensitive role of ASICs in the brain is still not known, although ASIC1a is a
177 predominant acid sensor modulating neural activity in physiological and pathological
178 conditions (18, 19). Here we demonstrated low-intensity ultrasound could modulate
179 neural activity in mouse brain and directly activate neurons (Fig. 1) via an ASIC1a-
180 depenent manner (Fig. 2-3). Moreover, repeated transcranial low-intensity
181 ultrasound stimulations are safe and able to elicit adult neurogenesis in mouse brains
182 (Fig. 4).

183 Although ASIC1a was determined as the molecular determinant involved in low-
184 intensity ultrasound mechanotransduction, non-selective mechanosensor inhibitors
185 such as gadolinium and ruthenium red were partially suppressing the calcium
186 response triggered by micropipette ultrasound (Fig. 2 *G* and *H*). Of note gadolinium
187 also blocked ASICs in μM to mM ranges. However, we cannot rule out a role of TRP
188 channels in the micropipette ultrasound mechanotransduction, because there is no
189 evidence showing ruthenium can also inhibit ASICs. Previous studies have proposed a
190 role of TRP for ultrasound-mediated mechanotransduction while high-intensity
191 ultrasound was applied. More studies are required to validate the role of TRP in low-
192 intensity ultrasound mechanotransdcution or the unexpected role of ruthenium red
193 in neuronal ASIC1a signaling pathways.

194 ASIC1a is widely expressed in the brain and could form as homotrimeric and
195 heterotrimeric channels with different sensitivity to PcTx1 inhibition (20, 21).
196 Specifically, heterotrimeric ASIC2b/ASIC1a can be inhibited 50% by approximately 3
197 nM (21) PcTx1 and ASIC1a/ASIC2a heterotrimeric can be inhibited by 50 nM(20)
198 whereas 0.5 nM to 1 nM can inhibit the homotrimeric ASIC1a (22, 23). Therefore,
199 since PcTx1 in low-doses effectively inhibited ASIC1a-mediated calcium signal by
200 micropipette ultrasound, homotrimeric ASIC1a channels may be the predominant
201 subtype involved in ultrasound mechanotransduction in cortical neurons (Fig. 3 *A* and
202 *SI Appendix,* Fig. S6).

203 To explain how ultrasound could activate ASIC1a via the tether-mode
204 mechanotransduction, we hypothesized a physical effect of micropipette ultrasound
205 at cell level; which the acoustic streaming imposes shear stress on cell apical surfaces
206 while ultrasound exerts compressional stresses throughout the cells. Considering the
207 tether model *in vitro*, we argue, in a mixed loading condition (Fig. 2 *B* and 3 *F*), the
208 extracellular domains of ASIC1a are under shear force pulling the protein to the flow

209 direction while the intracellular domains of the ASIC1a are connected to cortical
210 actin or other cytoskeleton, which experiences dynamic reorganization coupling with
211 membrane withdrawals in response to ultrasound (24). The anchor-pulling condition
212 *in vivo* on the other hand (*SI Appendix,* Fig. S6 *J*), is accomplished differently. Neurons
213 are embedded in extracellular matrixes (earthy yellow color) such as laminin, poly-
214 lysine, or poly-ornithine in the brain. When ultrasound is applied to the brain,
215 extracellular matrixes anchor the ASIC1a (earthy arrow) while cytoskeletal changes
216 pull it in a different direction (purple arrow), causing an activation of the cells
217 manifesting as ERK phosphorylation.

218 Since DCX has been accepted as a neurogenesis markers in dentate gyrus (14,
219 25), increased DCX-positive cells in dentate gyrus with a consecutive 3-day of
220 ultrasound treatment suggests a therapeutic implication. Of note, DCX plays multiple
221 roles in brain development including hippocampal pyramidal neuronal lamination,
222 cortical neuronal migration and axonal wiring (13, 26). The use of ultrasound in
223 developing brains should be extremely cautious.

224 In conclusion, here we provide evidence that a clinically safely low-intensity
225 transcranial ultrasound could modulate neuronal activity in mouse brain. The low-
226 intensity ultrasound can directly activate neurons via tether-mode
227 mechanotransduction and ASIC1a, which provides a molecular basis for future
228 development of ultrasound neuromodulation.

229

230 **References**

231 1. A. Cammalleri, P. Croce, W. Lee, K. Yoon, S. S. Yoo, Therapeutic Potentials of
232 Localized Blood-Brain Barrier Disruption by Noninvasive Transcranial Focused
233 Ultrasound: A Technical Review. *J Clin Neurophysiol* **37**, 104-117 (2020).
234 2. N. E. Nicodemus *et al.*, Focused transcranial ultrasound for treatment of
235 neurodegenerative dementia. *Alzheimers Dement (N Y)* **5**, 374-381 (2019).

236 3. W. Legon *et al.*, Transcranial focused ultrasound modulates the activity of
237 primary somatosensory cortex in humans. *Nat Neurosci* **17**, 322-329 (2014).
238 4. D. M. Panczykowski, E. A. Monaco, 3rd, R. M. Friedlander, Transcranial
239 focused ultrasound modulates the activity of primary somatosensory cortex
240 in humans. *Neurosurgery* **74**, N8 (2014).
241 5. T. Sato, M. G. Shapiro, D. Y. Tsao, Ultrasonic Neuromodulation Causes
242 Widespread Cortical Activation via an Indirect Auditory Mechanism. *Neuron*
243 **98**, 1031-1041 e1035 (2018).
244 6. S. Ibsen, A. Tong, C. Schutt, S. Esener, S. H. Chalasani, Sonogenetics is a non-
245 invasive approach to activating neurons in Caenorhabditis elegans. *Nat*
246 *Commun* **6** (2015).
247 7. Z. Qiu *et al.*, The Mechanosensitive Ion Channel Piezo1 Significantly Mediates
248 In Vitro Ultrasonic Stimulation of Neurons. *iScience* **21**, 448-457 (2019).
249 8. Y. R. Cheng, B. Y. Jiang, C. C. Chen, Acid-sensing ion channels: dual function
250 proteins for chemo-sensing and mechano-sensing. *J Biomed Sci* **25**, 46 (2018).
251 9. S. E. Murthy, A. E. Dubin, A. Patapoutian, Piezos thrive under pressure:
252 mechanically activated ion channels in health and disease. *Nat Rev Mol Cell*
253 *Biol* **18**, 771-783 (2017).
254 10. B. Nilius, E. Honore, Sensing pressure with ion channels. *Trends Neurosci* **35**,
255 477-486 (2012).
256 11. Y. J. Gao, R. R. Ji, c-Fos and pERK, which is a better marker for neuronal
257 activation and central sensitization after noxious stimulation and tissue
258 injury? *Open Pain J* **2**, 11-17 (2009).
259 12. Y. W. Lin, C. M. Cheng, P. R. Leduc, C. C. Chen, Understanding sensory nerve
260 mechanotransduction through localized elastomeric matrix control. *Plos One*
261 **4**, e4293 (2009).
262 13. J. Germain *et al.*, Doublecortin knockout mice show normal hippocampal-
263 dependent memory despite CA3 lamination defects. *Plos One* **8**, e74992
264 (2013).
265 14. K. Jin, X. Wang, L. Xie, X. O. Mao, D. A. Greenberg, Transgenic ablation of
266 doublecortin-expressing cells suppresses adult neurogenesis and worsens
267 stroke outcome in mice. *Proc Natl Acad Sci U S A* **107**, 7993-7998 (2010).
268 15. M. S. Rao, A. K. Shetty, Efficacy of doublecortin as a marker to analyse the
269 absolute number and dendritic growth of newly generated neurons in the
270 adult dentate gyrus. *Eur J Neurosci* **19**, 234-246 (2004).
271 16. S. H. Lin *et al.*, Evidence for the involvement of ASIC3 in sensory
272 mechanotransduction in proprioceptors. *Nat Commun* **7**, 11460 (2016).

273 17. C. C. Chen, C. W. Wong, Neurosensory mechanotransduction through acid-
274 sensing ion channels. *J Cell Mol Med* **17**, 337-349 (2013).
275 18. A. Baron, E. Lingueglia, Pharmacology of acid-sensing ion channels -
276 Physiological and therapeutical perspectives. *Neuropharmacology* **94**, 19-35
277 (2015).
278 19. J. A. Wemmie, R. J. Taugher, C. J. Kreple, Acid-sensing ion channels in pain
279 and disease. *Nat Rev Neurosci* **14**, 461-471 (2013).
280 20. N. Joeres, K. Augustinowski, A. Neuhof, M. Assmann, S. Grunder, Functional
281 and pharmacological characterization of two different ASIC1a/2a heteromers
282 reveals their sensitivity to the spider toxin PcTx1. *Sci Rep* **6**, 27647 (2016).
283 21. T. W. Sherwood, K. G. Lee, M. G. Gormley, C. C. Askwith, Heteromeric acid-
284 sensing ion channels (ASICs) composed of ASIC2b and ASIC1a display novel
285 channel properties and contribute to acidosis-induced neuronal death. *J*
286 *Neurosci* **31**, 9723-9734 (2011).
287 22. P. Escoubas, C. Bernard, G. Lambeau, M. Lazdunski, H. Darbon, Recombinant
288 production and solution structure of PcTx1, the specific peptide inhibitor of
289 ASIC1a proton-gated cation channels. *Protein Sci* **12**, 1332-1343 (2003).
290 23. N. J. Saez *et al.*, A dynamic pharmacophore drives the interaction between
291 Psalmotoxin-1 and the putative drug target acid-sensing ion channel 1a. *Mol*
292 *Pharmacol* **80**, 796-808 (2011).
293 24. Y. C. Chu, J. Lim, C. W. Hong, Y. S. Chu, J. L. Wang, Design of an ultrasound
294 chamber for cellular excitation and observation. *J Acoust Soc Am* **145**, EL547
295 (2019).
296 25. R. Salvi *et al.*, Distinct Effects of Chronic Dopaminergic Stimulation on
297 Hippocampal Neurogenesis and Striatal Doublecortin Expression in Adult
298 Mice. *Front Neurosci* **10**, 77 (2016).
299 26. H. Koizumi, T. Tanaka, J. G. Gleeson, Doublecortin-like kinase functions with
300 doublecortin to mediate fiber tract decussation and neuronal migration.
301 *Neuron* **49**, 55-66 (2006).

302

303 **Figure legend**

304 **Fig. 1.** Transcranial ultrasound induces pERK expression in neurons of the cortex,
305 hippocampus and amygdala of mouse brain. (*A*) Illustration depicting mouse head
306 stimulated by 1 MHz transducer which was positioned in between the mouse nasal
307 process of maxilla and the axis of mouse ear of an anesthetized mouse. (*B*)

308 Micrograph representing cortical region with basal level of p-ERK staining in sham
309 control mice (n=5), scale bar 100 μm. Sham control mice were handled with similar
310 procedures of placing transducer on the head without turning on the ultrasound
311 function generator. (*C*) Micrograph representing cortical region with p-ERK staining
312 stimulated by ultrasound (I_{SPTA}=5mW/cm^2, 1 minute) (n=5). (*D*) Quantitative bar
313 graph of the number of p-ERK stained cells within comparable area of 1.224mm^2
314 (Length 1275μm, Width 960μm), showing significant difference (p=0.0007) of cell
315 count by ImageJ. (*E*) Micrograph representing hippocampal region with basal level of
316 p-ERK staining in sham control mice. (*F*) Micrograph representing hippocampal
317 region with p-ERK staining in mice stimulated by ultrasound. (*G*) Bar graph showing
318 quantification of significantly p-ERK different cell count (1.224mm^2) (p=0.0132) in
319 hippocampal region. (*H*) Micrograph representing amygdala of sham controls. Scale
320 bar 100 μm (*I*) Micrograph representing amygdala of ultrasound stimulated mice. (*J*)
321 Quantification of amygdaloid significant difference (p=0.0023) of p-ERK cell count
322 (1.224mm^2).
323 **Fig. 2.** Neuronal calcium signals induced by micropipette-guided ultrasound
324 suppressed by ASIC1a inhibitors. (*A*) A micropipette positioned to the cortical
325 neurons cultured on a 30mm cover slips mounted to a chamber coupled to
326 microscope platform. Calcium signals recorded from neurons stained by Invitrogen™
327 Oregon Green™ 488 BAPTA-1, AM cell permeant. (*B*) Line graphs of averaged calcium
328 signals in 4 neurons stimulated by micropipette ultrasound for 3 seconds with an
329 input voltage 2000mVpp, duty factor (DF) 0.05%; or 100mVpp, DF100% or 700mVpp,
330 DF20%. The red-dotted line denotes start of the stimulation while the yellow-dotted
331 line denotes the end. (*C*) Calcium responses as a function of micropipette ultrasound
332 in 20%DF. Dose-dependent (input voltages from 10mVpp, to 900mVpp, DF20%)
333 responses of ultrasound with an EC50 of 700mVpp is shown (n=5). (*D*) Effects of

334 gadolinium (120 μM), a non-selective blocker of mechanically sensitive ion channels,
335 on calcium signals in cortical neurons. (*E*) Effects of GsMTx-4 (500nM), a selective
336 Piezo inhibitor, on calcium signals in cortical neurons. (*F*) Effects of Ruthenium red
337 (10 μM), a non-selective TRP inhibitor, on calcium signals in cortical neurons. (*G*)
338 Effects of amiloride (100 μm), an ASICs family inhibitor, on calcium signals in cortical
339 neurons. (*H*) Effects of PcTx1 treated (50 nM), a selective ASIC1a inhibitor, on calcium
340 signals in cortical neurons. (*I*) Statistical analyses of channel blockers on ultrasound-
341 induced calcium signals in cortical neurons.
342 **Fig. 3.** ASIC1a as a mechanoreceptor responsive to mechanical stimuli with combined
343 ultrasound and acoustic streaming. (*A*) PcTx1 dose-dependent inhibition curve of
344 calcium responses induced by micropipette ultrasound of 700mVpp, DF20% for 3-
345 second. (*B*) Whisker plots showing comparison of peak $\Delta F/F_0$ within 3-5 seconds
346 upon micropipette ultrasound (700mVpp, DF20%, 3-second) stimulation in the
347 untreated control primary neurons, 2- or 5mM EGTA treated neurons, RyR inhibitor
348 JTV519 fumarate (10 μM) treated neurons, or IP_3R inhibitor (-)-Xestonspongin C (1
349 μM) treated neurons. Student t-test with *p* value compared to control listed above
350 the whisker plot. (*C*) Graph showing calcium response of actin polymerization
351 inhibitor Cytochalasin D (5-10 μg/ml) treated neurons compared to untreated
352 control. (*D*) Calcium signals showing the effect of the microtubule assembly inhibitor
353 nocodazole (5-10 μg/ml) on neurons. (*E*) Whisker plots showing comparison of peak
354 $\Delta F/F_0$ within 3-5 seconds upon micropipette ultrasound (700mVpp, DF20%, 3-
355 second) stimulation in the untreated control primary neurons, cytochalasin D 5- or 10
356 μg/ml treated neurons, nocodazole 5- or 10 μg/ml treated neurons. Statistical *p*
357 values of one-way ANOVA analysis were listed to show the significance of treatment.
358 (*F*) Cartoon depicting ultrasound stimulating ASIC1a in the cell body of a neuron
359 under the micropipette ultrasound stimulation. Green arrow represents the pulling

360 force of acoustic stream and purple arrow represents the compression force of
361 ultrasound that results in cytoskeletal rearrangement.
362 **Fig. 4.** Neurogenesis in dentate gyrus induced by repeated transcranial ultrasound
363 treatments. (*A*) The mice were treated 3 consecutive days by ultrasound of
364 4mW/cm^2, 1% for 5 minutes, subsequently perfused fixed at day 4 or day 7 and
365 brains were dissected from the head and sectioned for immunofluorescence
366 procedures. The DCX staining in dentate gyrus of treated mice were compared to
367 control untreated one. (*B*) Cell count with clear DAPI stained nucleus surrounded by
368 DCX markers compared in control, day 4 and day 7 post-ultrasound treatments.
369 Statistical analysis: p=0.0013 and F ratio=15.18 in one-way ANOVA (n=4). (*C, D*)
370 Representative micrograph of untreated mice. The vibratome coronal brain sections
371 (100 μm) of dentate gyrus region immunofluorescently stained for DCX (green) and
372 MAP2 (red). Blue color indicates DAPI stained nuclei. Representative micrograph
373 showing. (*E, F*) Representative micrograph from ultrasound treated mice fixed at day
374 4. (*G, H*) Representative micrograph from ultrasound treated mice fixed at day

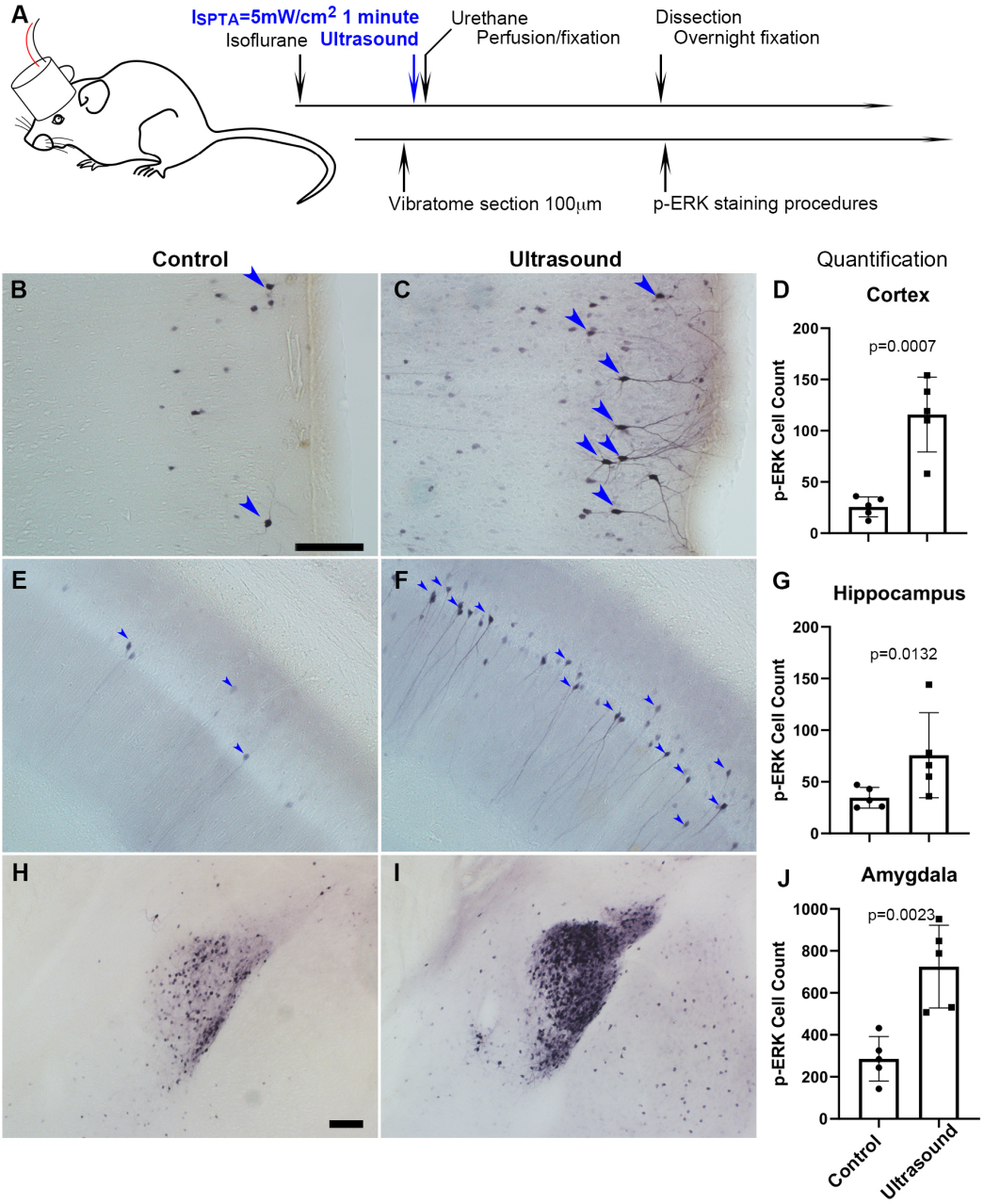
A
ISPTA=5mW/cm2 1 minute
Isoflurane
Ultrasound
Urethane
Perfusion/fixation
Dissection
Overnight fixation
Vibratome section 100μm
p-ERK staining procedures
Control
Ultrasound
Quantification
B
C
D
Cortex
p=0.0007
p-ERK Cell Count
E
F
G
Hippocampus
p=0.0132
H
I
J
Amygdala
p=0.0023
Control
Ultrasound

375

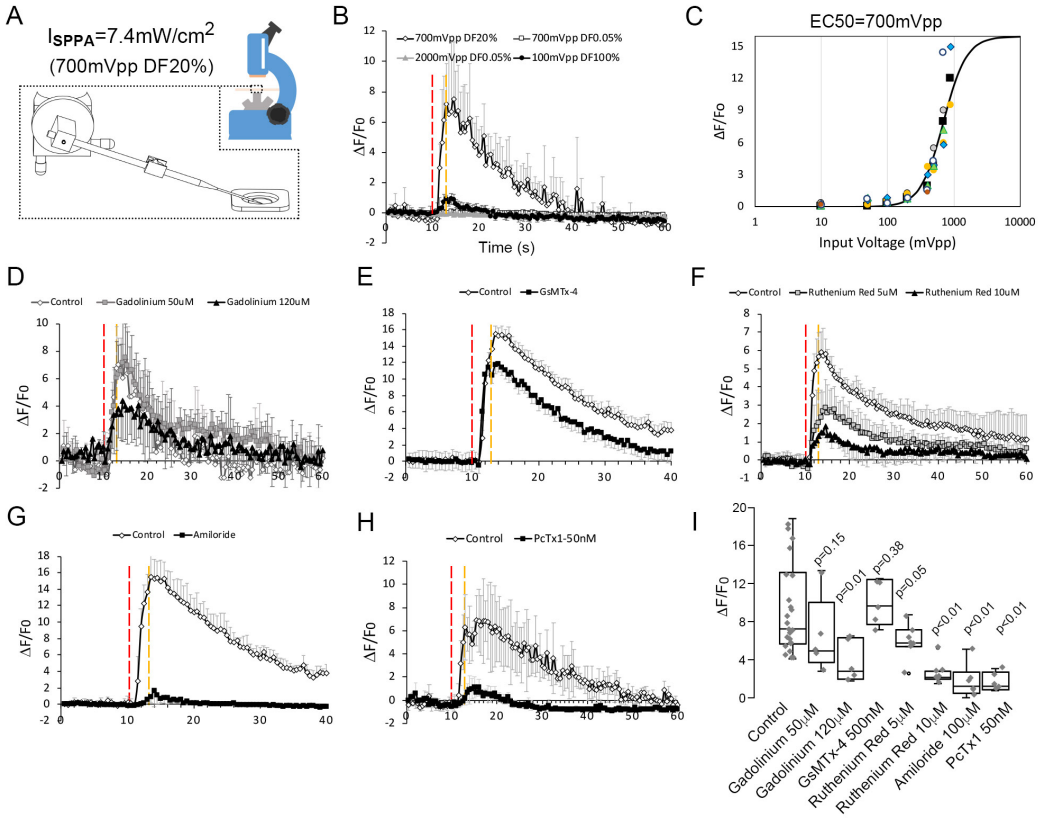
A
ISPPA=7.4mW/cm2
(700mVpp DF20%)
B
700mVpp DF20%
700mVpp DF0.05%
2000mVpp DF0.05%
100mVpp DF100%
ΔF/Fo
Time (s)
C
EC50=700mVpp
ΔF/Fo
Input Voltage (mVpp)
D
Control
Gadolinium 50uM
Gadolinium 120uM
ΔF/Fo
E
Control
GsMTx-4
ΔF/Fo
F
Control
Ruthenium Red 5uM
Ruthenium Red 10uM
ΔF/Fo
G
Control
Amiloride
ΔF/Fo
H
Control
PcTx1-50nM
ΔF/Fo
I
ΔF/Fo
p=0.15
p=0.01
p=0.38
p=0.05
p<0.01
p<0.01
p<0.01
Control
Gadolinium 50μM
Gadolinium 120μM
GsMTx-4 500nM
Ruthenium Red 5μM
Ruthenium Red 10μM
Amiloride 100μM
PcTX1 50nM

376

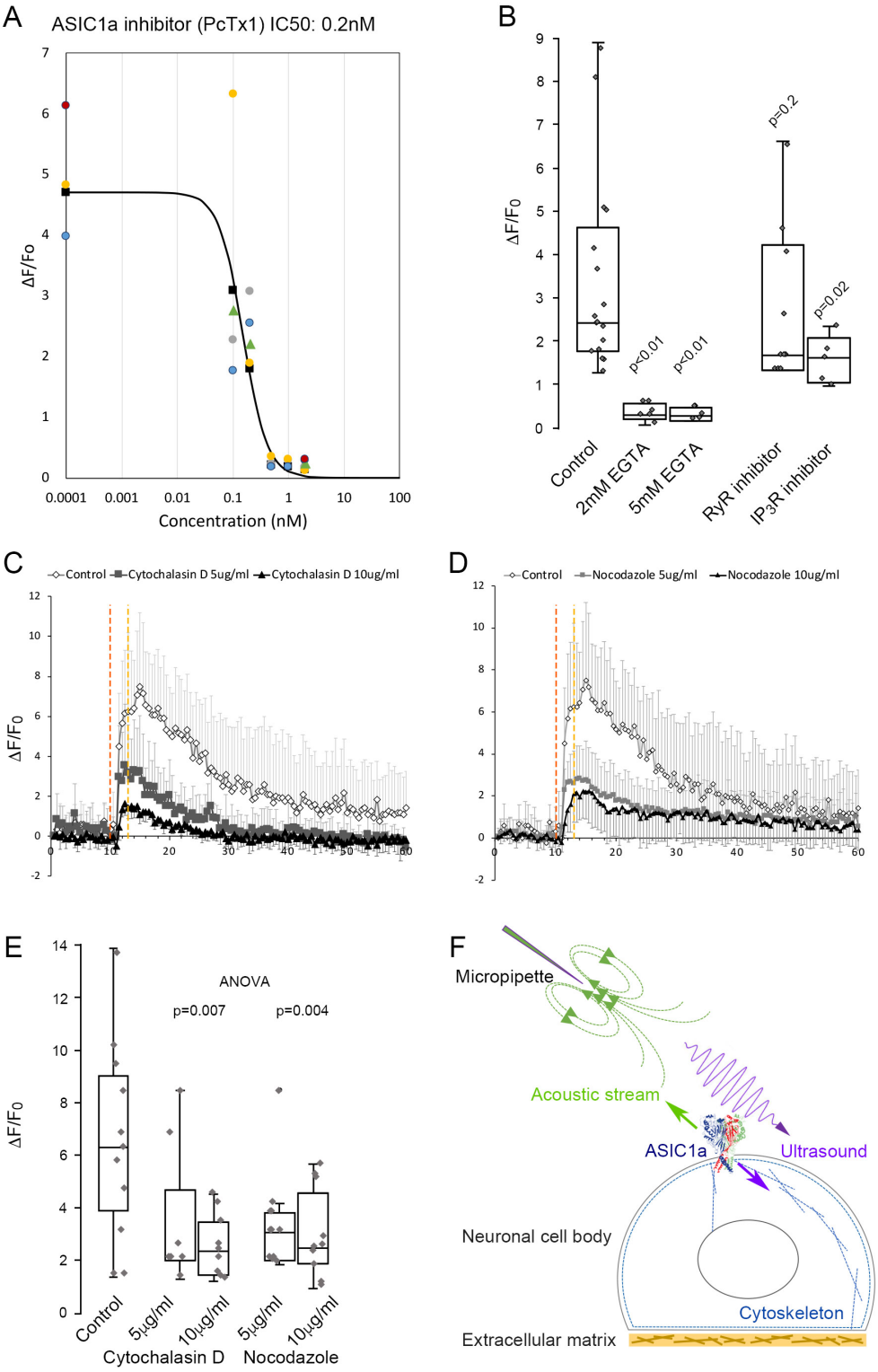
A
ASIC1a inhibitor (PcTx1) IC50: 0.2nM
ΔF/Fo
Concentration (nM)
B
ΔF/F0
p<0.01
p<0.01
p=0.2
p=0.02
Control
2mM EGTA
5mM EGTA
RyR inhibitor
IP3R inhibitor
C
Control
Cytochalasin D 5ug/ml
Cytochalasin D 10ug/ml
ΔF/F0
D
Control
Nocodazole 5ug/ml
Nocodazole 10ug/ml
E
ANOVA
p=0.007
p=0.004
ΔF/F0
Control
5μg/ml
10μg/ml
5μg/ml
10μg/ml
Cytochalasin D
Nocodazole
F
Micropipette
Acoustic stream
ASIC1a
Ultrasound
Neuronal cell body
Cytoskeleton
Extracellular matrix

377

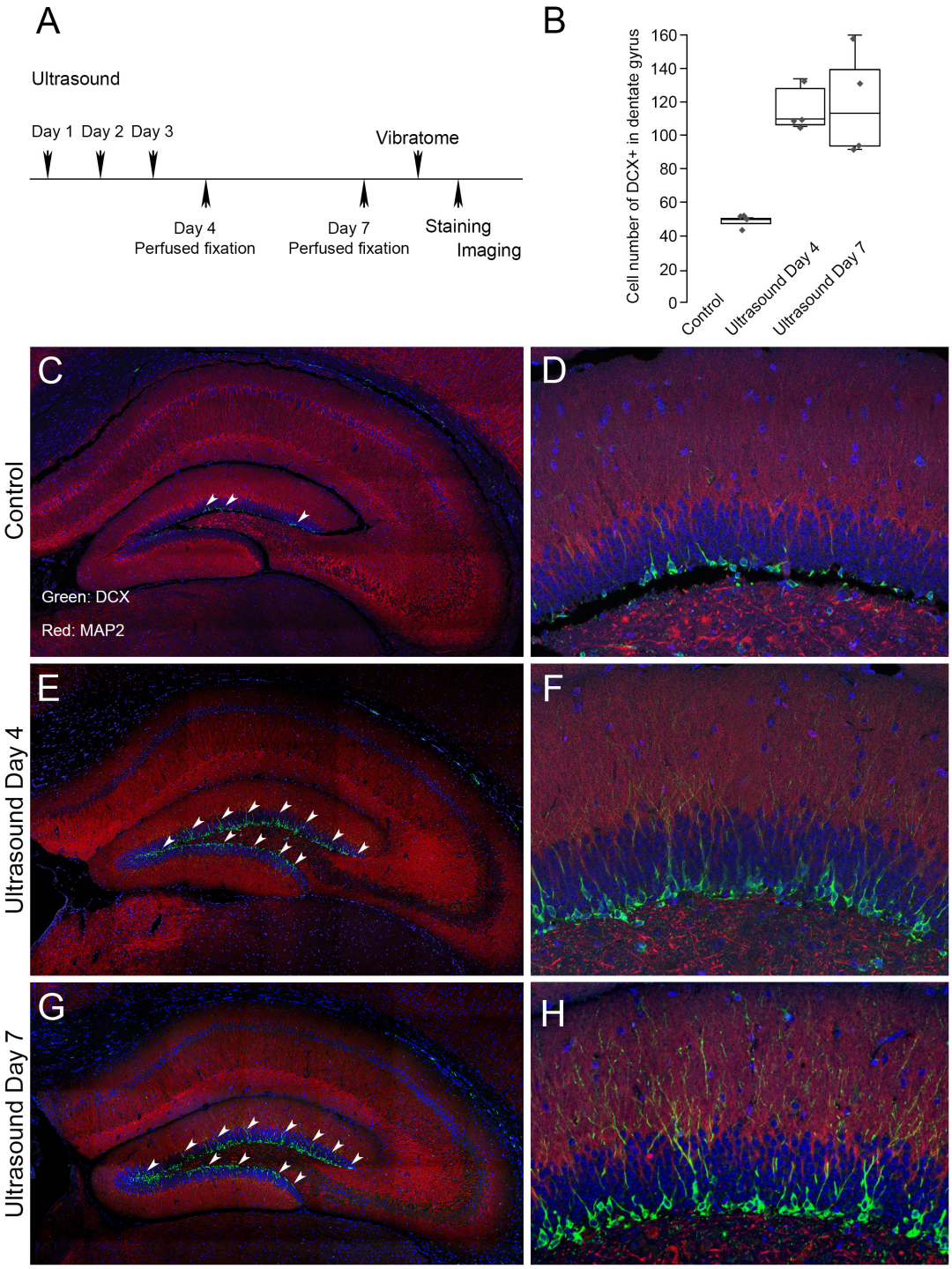
A
Ultrasound
Day 1 Day 2 Day 3
Vibratome
Day 4
Perfused fixation
Day 7
Perfused fixation
Staining
Imaging
B
Cell number of DCX+ in dentate gyrus
160
140
120
100
80
60
40
20
0
Control
Ultrasound Day 4
Ultrasound Day 7
C
D
E
F
G
H
Control
Ultrasound Day 4
Ultrasound Day 7
Green: DCX
Red: MAP2

378

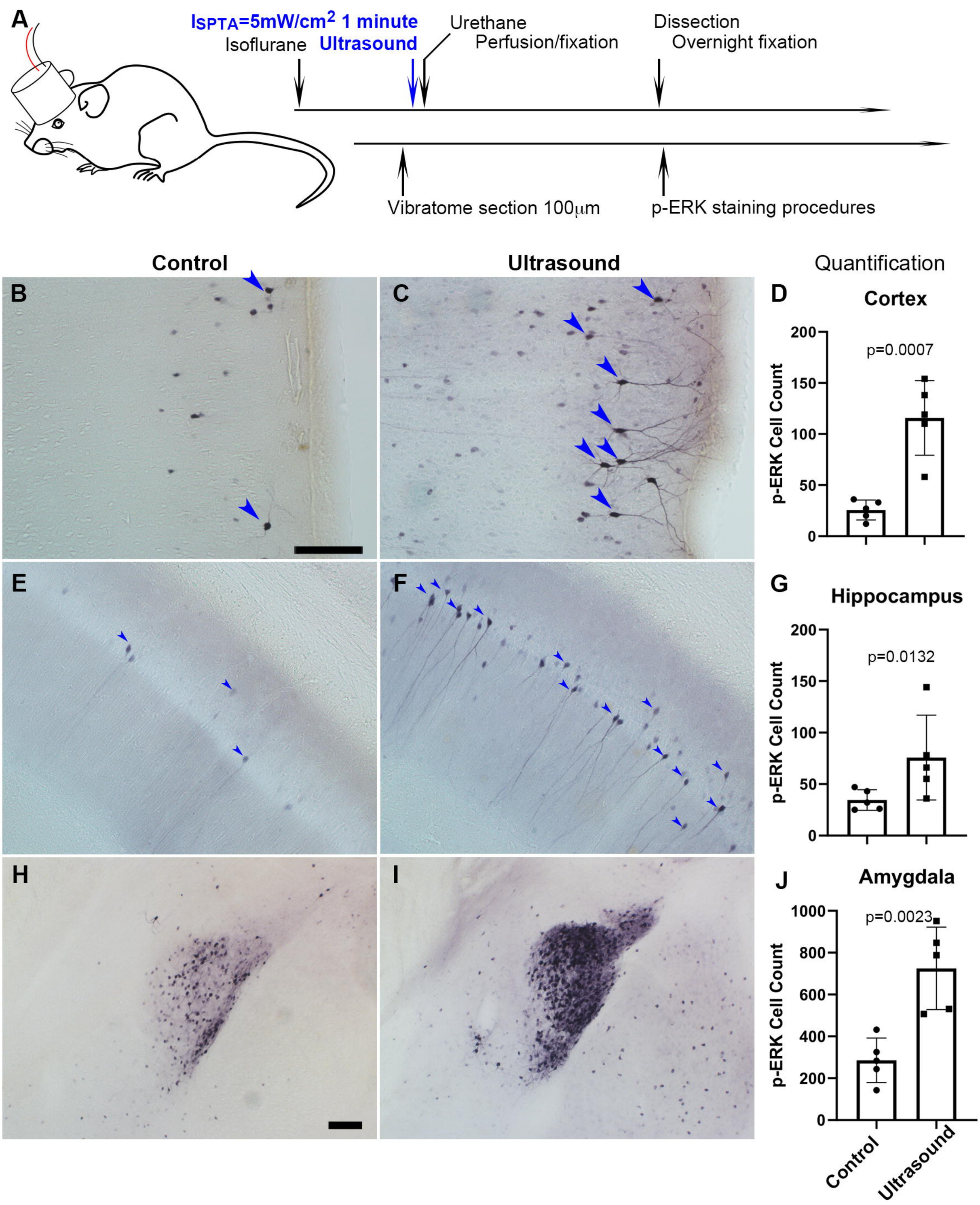
A
ISPTA=5mW/cm2 1 minute
Isoflurane
Ultrasound
Urethane
Perfusion/fixation
Dissection
Overnight fixation
Vibratome section 100μm
p-ERK staining procedures
Control
Ultrasound
Quantification
B
C
D
Cortex
p=0.0007
p-ERK Cell Count
200
150
100
50
0
E
F
G
Hippocampus
p=0.0132
p-ERK Cell Count
200
150
100
50
0
H
I
J
Amygdala
p=0.0023
p-ERK Cell Count
1000
800
600
400
200
0
Control
Ultrasound

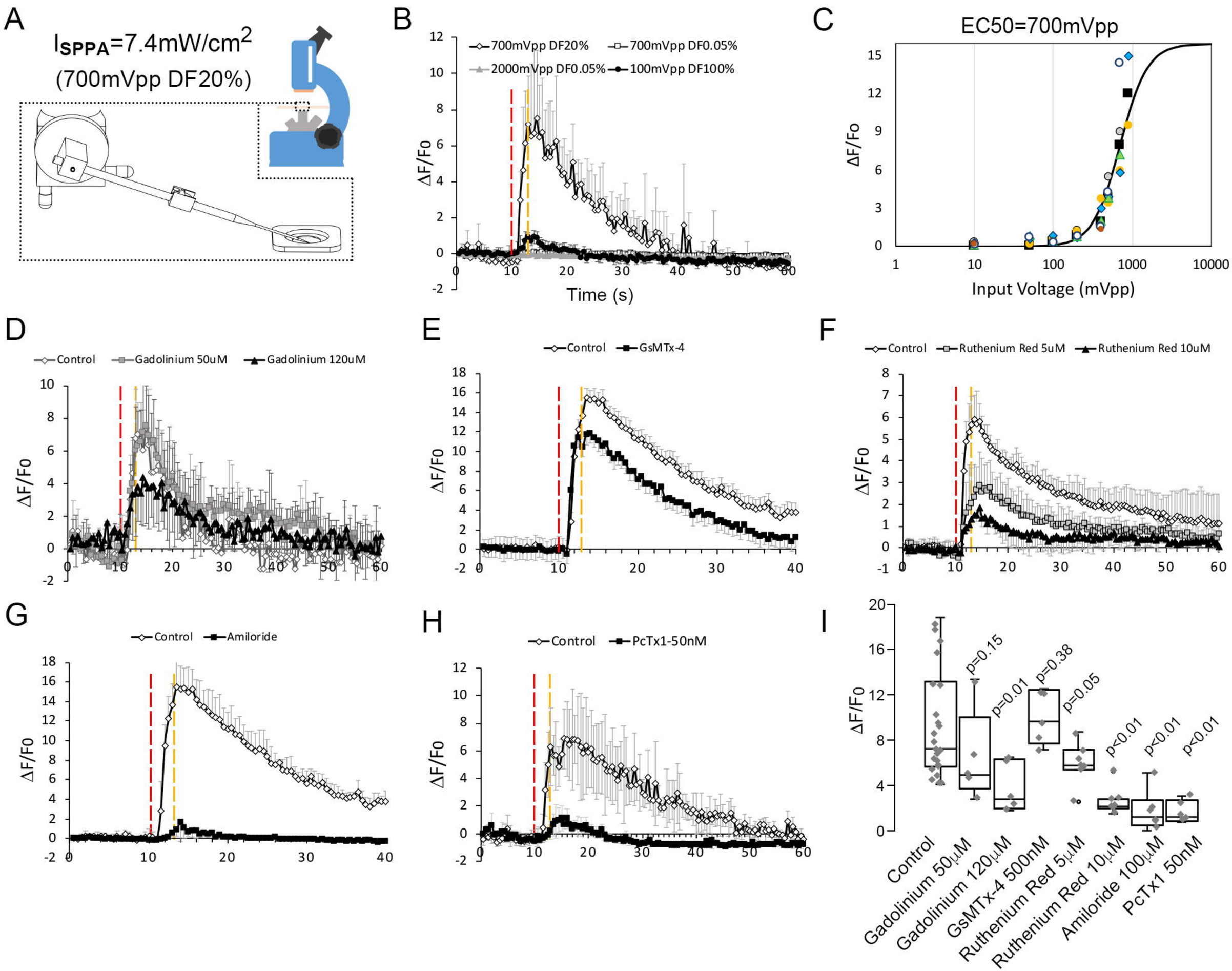
A
I_{SPPA}=7.4mW/cm^2
(700mVpp DF20%)
B
700mVpp DF20%
700mVpp DF0.05%
2000mVpp DF0.05%
100mVpp DF100%
ΔF/F0
Time (s)
C
EC50=700mVpp
ΔF/Fo
Input Voltage (mVpp)
D
Control
Gadolinium 50uM
Gadolinium 120uM
ΔF/F0
E
Control
GsMTx-4
ΔF/F0
F
Control
Ruthenium Red 5uM
Ruthenium Red 10uM
ΔF/F0
G
Control
Amiloride
ΔF/F0
H
Control
PcTx1-50nM
ΔF/F0
I
ΔF/F0
p=0.15
p=0.01
p=0.38
p=0.05
p<0.01
p<0.01
p<0.01
Control
Gadolinium 50μM
Gadolinium 120μM
GsMTx-4 500nM
Ruthenium Red 5μM
Ruthenium Red 10μM
Amiloride 100μM
PcTx1 50nM

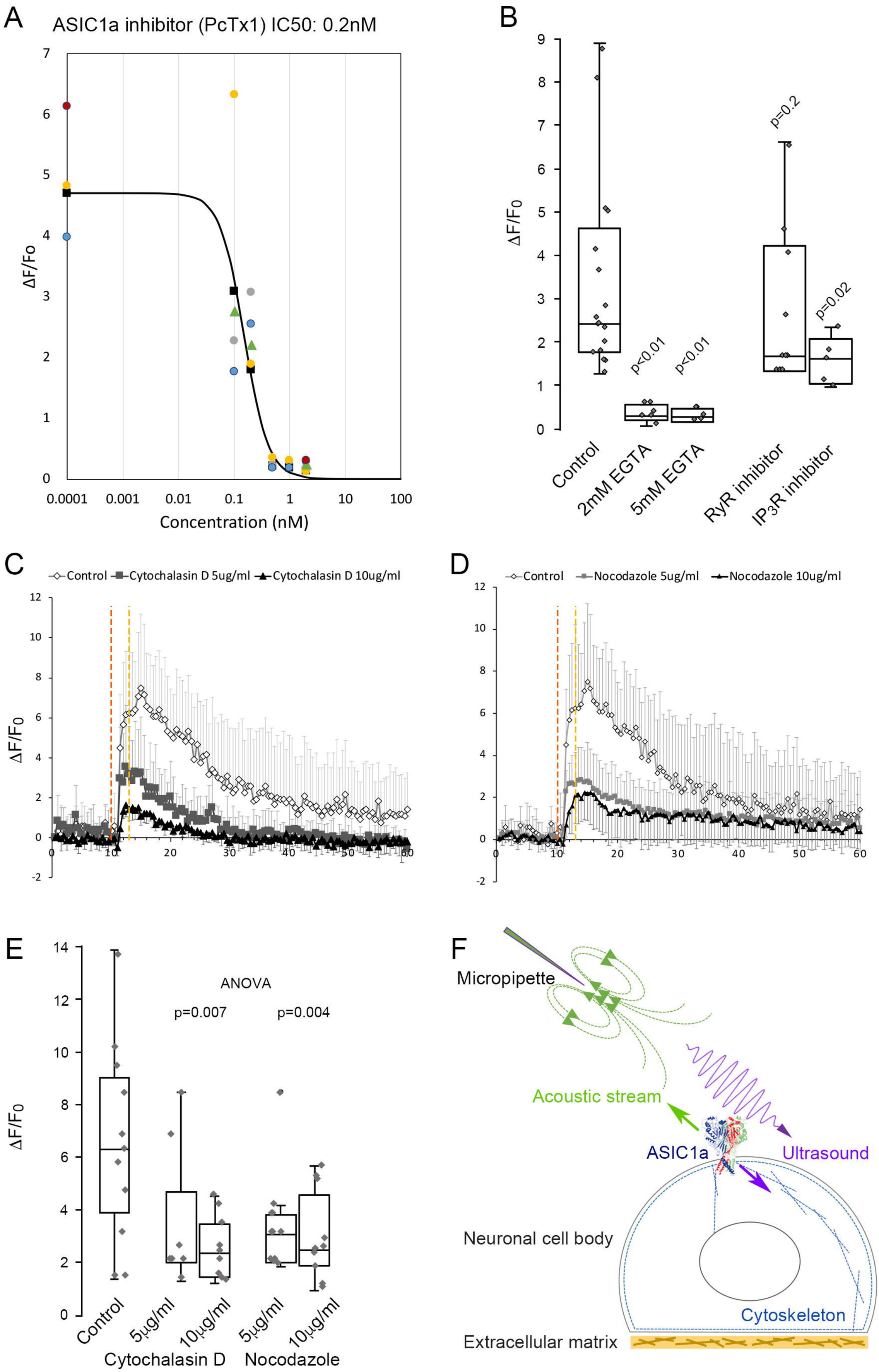
A
ASIC1a inhibitor (PcTx1) IC50: 0.2nM
ΔF/Fo
Concentration (nM)
B
ΔF/F0
p<0.01
p<0.01
p=0.2
p=0.02
Control
2mM EGTA
5mM EGTA
RyR inhibitor
IP3R inhibitor
C
Control
Cytochalasin D 5ug/ml
Cytochalasin D 10ug/ml
ΔF/F0
D
Control
Nocodazole 5ug/ml
Nocodazole 10ug/ml
E
ANOVA
p=0.007
p=0.004
ΔF/F0
Control
5μg/ml
10μg/ml
5μg/ml
10μg/ml
Cytochalasin D
Nocodazole
F
Micropipette
Acoustic stream
ASIC1a
Ultrasound
Neuronal cell body
Cytoskeleton
Extracellular matrix

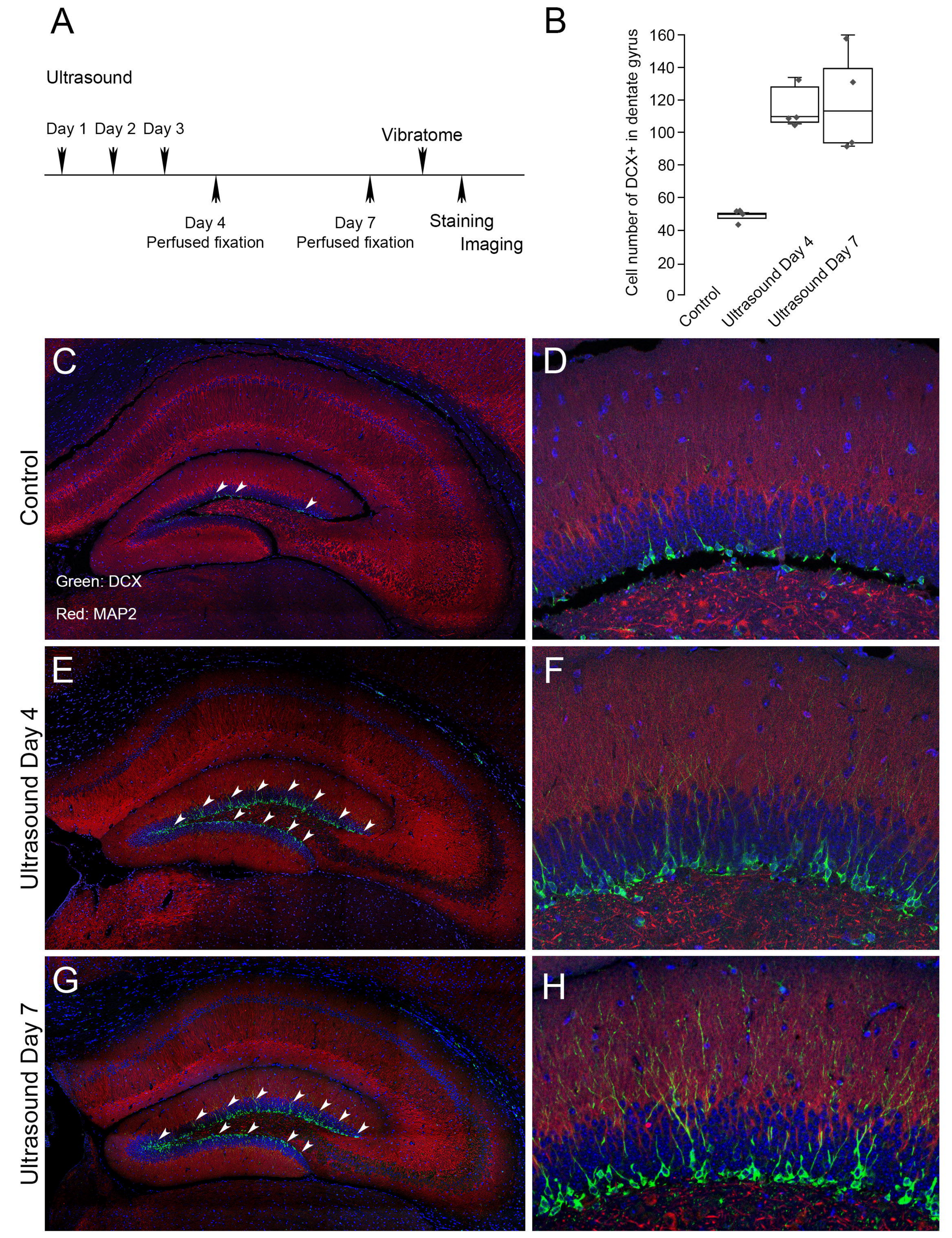
A
Ultrasound
Day 1
Day 2
Day 3
Vibratome
Day 4
Perfused fixation
Day 7
Perfused fixation
Staining
Imaging
B
Cell number of DCX+ in dentate gyrus
160
140
120
100
80
60
40
20
0
Control
Ultrasound Day 4
Ultrasound Day 7
C
D
Control
Green: DCX
Red: MAP2
E
F
Ultrasound Day 4
G
H
Ultrasound Day 7